RESEARCH ARTICLE SUMMARY

ATMOSPHERE

Toward a Cenozoic history of atmospheric CO_2

The Cenozoic CO_2 Proxy Integration Project ($CenCO_2PIP$) Consortium

INTRODUCTION: Anthropogenic carbon dioxide (CO_2) emissions have driven an increase in the global atmospheric CO_2 concentration from 280 parts per million (ppm) before industrialization to an annual average of 419 ppm in 2022, corresponding to an increase in global mean surface temperature (GMST) of 1.1°C over the same period. If global CO_2 emissions continue to rise, atmospheric CO_2 could exceed 800 ppm by the year 2100. This begs the question of where our climate is headed. The geologic record is replete with both brief and extended intervals of CO_2 concentration higher than today and thus provides opportunities to project the response of the future climate system to increasing CO_2. For example, it has been estimated that global surface temperature 50 million years ago (Ma) was ~12°C higher than today, in tandem with atmospheric CO_2 concentrations some 500 ppm higher (i.e., more than doubled) than present-day values. Consistent with these estimates, Antarctica and Greenland were free of ice at that time. However, reconstructing these values prior to direct instrumental measurements requires the use of paleoproxies—measurable properties of geological archives that are closely, but only indirectly, related to the parameter in question (e.g., temperature, CO_2). To date, at least eight different proxies from both terrestrial and marine archives have been developed and applied to reconstruct paleo-CO_2, but their underlying assumptions have been revised over time, and published reconstructions are not always consistent. This uncertainty complicates quantification of the climate responses to the ongoing rise of atmospheric CO_2 concentrations.

RATIONALE: Although earlier studies have compiled published paleo-CO_2 estimates, those studies typically applied only limited proxy vetting, included estimates that were made before the proxies were sufficiently validated, and/or focused on only a subset of available proxy data. The international consortium of the Cenozoic CO_2 Proxy Integration Project ($CenCO_2PIP$) has undertaken a 7-year effort to document, evaluate, and synthesize published paleo-CO_2 records from all available archives, spanning the past 66 million years. The most reliable CO_2 estimates were identified, some records were recalculated to conform with the latest proxy understanding, age models were updated where necessary and possible, and data were categorized according to the community's level of confidence in each estimate. The highest-rated data were eventually combined into a reconstruction of the Cenozoic history o mospheric CO_2.

RESULTS: The resulting reconstruction illustrates a more quantitatively robust relationship between CO_2 and global surface temperature, yielding greater clarity and confidence than previous syntheses. The new record suggests that early Cenozoic "hothouse" CO_2 concentrations peaked around 1600 ppm at ~51 Ma. Near 33.9 Ma, the onset of continent-wide Antarctic glaciation coincided with an atmospheric CO_2 concentration of 720 ppm. By ~32 Ma, atmospheric CO_2 had dropped to 550 ppm, and this value coincided with the onset of radiation in plants with carbon-concentrating mechanisms that populate grasslands and deserts today. CO_2 remained below this threshold for the remainder of the Cenozoic and continued its long-term decrease toward the present. Along this trajectory, the middle Miocene (~16 Ma) marks the last time that CO_2 concentrations were consistently higher than at present; Greenland was not yet glaciated at that time, and independent estimates suggest that sea level was some 50 m higher than today. Values eventually dropped below 270 ppm at the Plio-Pleistocene boundary (2.6 Ma), when Earth approached our current "icehouse" state of bipolar glaciation. This and other climatic implications of the revised CO_2 curve, including the evolution of the cryosphere, flora, and fauna, along with the cross-disciplinary data assessment process, are detailed in the full online article.

CONCLUSION: This community-vetted CO_2 synthesis represents the most reliable data available to date and a means to improve our understanding of past changes in global climate and carbon cycling as well as organismal evolution. However, this effort is still incomplete. Data remain sparse during the earlier part of the record and in some instances are dominated by estimates from a single proxy system. Generating a paleo-CO_2 record with even greater confidence will require further research using multiple proxies to fill in data gaps and increase overall data resolution, resolve discrepancies between estimates from contemporaneous proxy analyses, reduce uncertainty of established methods, and develop new proxies. ■

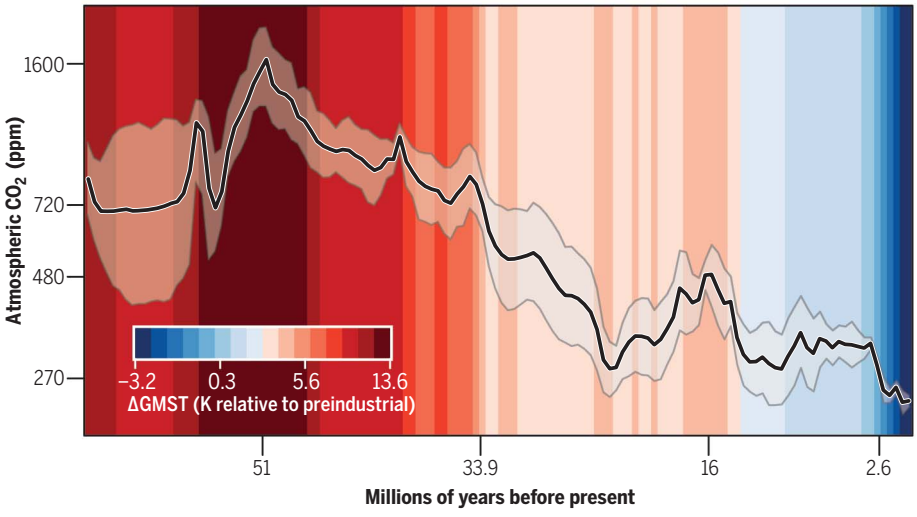

Community-vetted quantitative CO_2 record. Paleo-CO_2 (including 95% credible intervals) is superimposed on the GMST trend over the past 66 million years. Age and CO_2 labels highlight notable climate extrema and transitions as described in the text.

The $CenCO_2PIP$ Consortium authors and affiliations are listed in the full article online.
Corresponding authors: Bärbel Hönisch (hoenisch@ldeo.columbia.edu); Dana L. Royer (droyer@wesleyan.edu); Daniel O. Breecker (breecker@jsg.utexas.edu); Gabriel J. Bowen (gabe.bowen@utah.edu); Pratigya J. Polissar (polissar@ucsc.edu); Andy Ridgwell (andy@seao2.org)
Cite this article as The $CenCO_2PIP$ Consortium, *Science* **382**, eadi5177 (2023). DOI: 10.1126/science.adi5177

READ THE FULL ARTICLE AT
https://doi.org/10.1126/science.adi5177

RESEARCH ARTICLE

ATMOSPHERE

Toward a Cenozoic history of atmospheric CO_2

The Cenozoic CO_2 Proxy Integration Project ($CenCO_2PIP$) Consortium*†

The geological record encodes the relationship between climate and atmospheric carbon dioxide (CO_2) over long and short timescales, as well as potential drivers of evolutionary transitions. However, reconstructing CO_2 beyond direct measurements requires the use of paleoproxies and herein lies the challenge, as proxies differ in their assumptions, degree of understanding, and even reconstructed values. In this study, we critically evaluated, categorized, and integrated available proxies to create a high-fidelity and transparently constructed atmospheric CO_2 record spanning the past 66 million years. This newly constructed record provides clearer evidence for higher Earth system sensitivity in the past and for the role of CO_2 thresholds in biological and cryosphere evolution.

The contribution of atmospheric CO_2 to Earth's greenhouse effect and the potential for variations in the global carbon cycle to cause climate change have been known for more than a century (*1*), but it was only in 1958 that direct measurements of the concentration of CO_2 in the atmosphere (or molar mixing ratio—the mole fraction of a gas in one mole of air) were systematically collected. Alongside reconstructions of the historical rise in Earth's surface temperature (*2*), this record has become one of the most influential and scientifically valuable environmental time series, documenting the continuous rise in annual mean CO_2 from 315 parts per million (ppm) in 1958 to 419 ppm in 2022 (*3*). Projecting beyond these records to estimate how Earth's climate will respond to further increases in CO_2 requires global climate models (*4*). However, despite successfully explaining observed historical climate change (*2*), models leave doubt as to whether global mean temperature will rise linearly as a function of future doubling of CO_2 (an invariant "climate sensitivity") or whether climate feedbacks will lead to an increasing (or "state-dependent") sensitivity of climate to CO_2 in the future (*5*, *6*).

We can turn to the geological record to help constrain models and improve our understanding of nonlinearities in the climate system (*7*), as it documents a variety of global climate changes and, critically, climate states warmer than today. Leveraging this record, however, requires the paired quantification of both past atmospheric CO_2 and temperature. In parallel with recent efforts to compile and vet paleotemperature estimates (*8*), here we focus on paleo-CO_2 estimates. Samples of ancient air can be extracted and analyzed from bubbles preserved in ancient polar ice (*9*, *10*), but continuous ice core records currently only extend our knowledge of CO_2 back about 800 thousand years (kyr) [for a compilation, see (*11*)], with isolated time slices extending to ~2 Ma (million years ago) (*12*, *13*). Importantly, at no point during the Pleistocene (2.58 Ma to 11,700 years ago) did CO_2 come close to present-day values (419 ppm in the year 2022), with 300 ppm being the highest value measured to date (*14*). In contrast, depending on the extent of future human emissions, atmospheric CO_2 could reach between 600 and 1000 ppm by the year 2100 (*2*). Feedbacks between changing climate and the carbon cycle may also amplify or diminish emissions from surficial carbon reservoirs (e.g., thawing permafrost, adjustments in size and composition of the terrestrial biosphere and marine carbon pool), creating additional uncertainty in future CO_2 projections (*15*, *16*). Past changes in CO_2 inherently include the role of these feedbacks, and their study could help reduce uncertainty in Earth system models (*17*).

A solid understanding of atmospheric CO_2 variation through geological time is also essential to deciphering and learning from other features of Earth's history. Changes in atmospheric CO_2 and climate are suspected to have caused mass extinctions (*18*, *19*) but also evolutionary innovations (*20*, *21*). During the Cenozoic, long-term declines in CO_2 and associated climate cooling have been proposed as the drivers of changing plant physiology (e.g., carbon-concentrating mechanisms), species competition and dominance, and, relatedly, mammalian evolution. A more refined understanding of past trends in CO_2 is therefore central to understanding how modern species and ecosystems arose and may fare in the future.

Extending the CO_2 record beyond the temporally restricted availability of polar ice requires the use of "proxies." In essence, a CO_2 proxy could be any biological and/or geochemical property of a fossil or mineral that responds to the concentration of ambient CO_2 when it is formed. Unfortunately, unlike in the case of bubbles of ancient air trapped in polar ice, this response is invariably indirect. The connection between a proxy signal and atmospheric CO_2 is often strongly mediated by biological "vital effects" (e.g., concentration of or discrimination against certain molecules, elements, or isotopes as a result of physiological processes such as biomineralization, photosynthesis, respiration), may be indirectly connected to the atmosphere through dissolution of carbon in seawater or lakes, may involve isotopic or other chemical fractionation steps, or a combination of these. When preserved in terrestrial or marine sediments, proxy substrates can also be affected by postdepositional (i.e., diagenetic) processes that must be accounted for. Relationships between proxies and CO_2 are typically calibrated using observations or laboratory experiments; in biological systems, these calibrations are often limited to modern systems (e.g., modern organisms or soils), and applications to the distant past focus on physiologically or physically similar systems preserved in the sediment and rock record (e.g., similar fossil organisms or fossil soils). Most CO_2 proxies also require estimation of one or more additional environmental parameters and hence depend on additional proxy records. The complexity of proxy-enabled paleoclimate reconstructions thus presents a major challenge for creating a self-consistent estimate of atmospheric CO_2 through geological time and requires careful validation.

One of the first paleo-CO_2 proxies to be devised is based on the observation that vascular plants typically optimize the density, size, and opening and closing behavior of stomatal pores on their leaf surfaces to ensure sufficient CO_2 uptake while minimizing water loss (*22*). A count of stomatal frequencies then provides a simple proxy for the CO_2 concentration experienced by the plant (*23*). Changes in ambient CO_2 can also drive a cascade of interrelated effects on photosynthesis, the flux of CO_2 into the leaf (largely determined by stomatal size and density), and the carbon isotopic fractionation during photosynthesis ($\Delta^{13}C$) (*22*–*24*). Despite lacking functional stomata, nonvascular plants such as liverworts also exhibit isotopic fractionation during photosynthesis, and their $\delta^{13}C$ values are thus similarly controlled by ambient CO_2. The list of terrestrial paleo-CO_2 proxies also includes inorganic carbonate nodules precipitated in ancient soils (i.e., paleosols) and sodium carbonate minerals precipitated in continental lacustrine evaporites. Whereas the paleosol proxy uses the carbon isotope composition of carbonate nodules and deconvolves the mixture of atmospheric and soil-respired CO_2 in soil porewaters using models of soil CO_2 (*25*, *26*), the nahcolite

*Corresponding authors: Bärbel Hönisch (hoenisch@ldeo.columbia.edu); Dana L. Royer (droyer@wesleyan.edu); Daniel O. Breecker (breecker@jsg.utexas.edu); Gabriel J. Bowen (gabe.bowen@utah.edu); Pratigya J. Polissar (polissar@ucsc.edu); Andy Ridgwell (andy@seao2.org)
†The $CenCO_2PIP$ Consortium authors and affiliations are listed at the end of this paper.

proxy is based on the CO_2 dependence of sodium carbonate mineral equilibria (*27*, *28*). Analogously to nonvascular plants on land, phytoplankton fractionate carbon isotopes during photosynthesis in response to the concentration of dissolved CO_2 in seawater, creating an isotopic signal stored in organic biomolecules that can be retrieved from ocean sediments (*29*). Boron proxies recorded in fossil shells of marine calcifying organisms are related to seawater pH, which in turn can be related back to atmospheric CO_2 (*30*, *31*). An in-depth discussion of the analytical details, entrained assumptions, and inherent uncertainties of currently available CO_2 proxies, plus summaries of recent advances and opportunities for further validation, is presented in the supplementary materials and in table S1.

Although each of these proxies has been validated extensively, comparing reconstructions from different proxies often reveals discrepancies. Compilations of paleo-CO_2 and explorations of the CO_2-climate linkage already exist (*32*–*34*); however, those studies apply limited proxy vetting, include CO_2 estimates that predate major innovations in some methods, and use rather basic data interpolation to assess broad CO_2 trends. Earlier CO_2 reconstructions are also often insufficiently constrained by ancillary data (e.g., concomitant temperature, isotopic composition of seawater or atmosphere) to be consistent with modern proxy theory, have incomplete or missing uncertainty estimates for CO_2 and/or sample age, and may exhibit fundamental disagreement with other proxies, leaving our current understanding of past CO_2 concentrations incomplete.

Here we present the results of a 7-year endeavor by an international consortium of researchers whose collective expertise spans the reconstruction of paleo-CO_2 from all available terrestrial and marine archives. We have jointly created a detailed, open-source database of published paleo-CO_2 estimates including all raw and ancillary data together with associated analytical and computational methods. Each record was vetted and categorized in view of the most recent proxy understanding, with calculations adopting a common methodology including full propagation of uncertainties. We focused our efforts on the Cenozoic, when the spatial distribution of continents and ocean basins, as well as the structure of marine and terrestrial ecosystems, was similar to modern times, yet profound changes in CO_2 and climate occurred. Identifying the most-reliable Cenozoic CO_2 estimates published to date allows us to quantify important physical (e.g., temperature, ice volume) and biological (i.e., physiological, ecosystem) thresholds and tipping points.

We structure this investigation as follows: First we summarize the methodology by which we assessed the CO_2 proxies and associated estimates. We then apply these methods to derive a series of paleo-CO_2 compilations composed of data with different levels of quality or confidence, and we statistically integrate the "top-tier" data to create a realization of the Cenozoic variability in atmospheric CO_2. This is followed by a discussion of the climatic implications (including climate sensitivity) of the paleo-CO_2 curve and a presentation of an evolutionary perspective. We finish with a road map for further advances in understanding past changes in atmospheric CO_2.

Critical assessment of atmospheric CO_2 proxies

The basis of our synthesis is a set of comprehensive data templates documenting all types of proxy data and their corresponding CO_2 estimates (a total of 6247 data points). The completed data sheets for each study can be accessed as the paleo-CO_2 "Archive" (https://www1.ncdc.noaa.gov/pub/data/paleo/climate_forcing/trace_gases/Paleo-pCO2/) in the National Oceanic and Atmospheric Administration's National Centers for Environmental Information (NOAA NCEI). These "Archive" sheets report all underlying data at face value from the original publications, but their unprecedented level of detail is designed to facilitate critical evaluation and recalculation of each CO_2 estimate.

From the "Archive," published CO_2 estimates were evaluated by teams of experts—often including the original authors of the respective data—who are active in validating and applying these proxies. No new proxy data were collected as part of this effort, but estimates were recalculated where needed and possible, and age models were revised where new evidence was readily accessible. Additionally, CO_2 and age uncertainties were updated, as necessary, to consistently reflect propagated 95% confidence intervals (CIs). The vetting criteria are summarized in table S1 and detailed in paleo-CO_2 "Product" sheets (https://www.ncei.noaa.gov/pub/data/paleo/climate_forcing/trace_gases/Paleo-pCO2/product_files/). These CO_2 estimates are categorized as follows: "Category 1" estimates (Fig. 1A; 1673 data points or ~27% of the original total) are based on data whose uncertainty is fully documented and quantifiable in view of current proxy understanding. "Category 2" estimates (Fig. 1B; 1813 data points) contain sources of uncertainty that are not yet fully constrained. These uncertainties vary between proxies and datasets and include, for example, insufficient replication, poorly constrained proxy sensitivity to parameters other than CO_2, or extrapolation of calibration curves. "Category 3" estimates (the residual 2761 data points, or ~44% of the Cenozoic paleo-CO_2 estimates published to date) are either superseded by newer, independently published evaluations from the same raw data or are considered unreliable owing to factors such as incomplete supporting datasets, which prevent full quantification of uncertainties, or outdated sample preparation methods.

Although objective criteria are applied throughout, the vetting process was particularly challenging for the paleosol- and phytoplankton-based proxies because multiple approaches are currently in use for interpreting these proxy data (*35*–*41*). Given the lack of a universally agreed-upon method, we compared multiple approaches for treating the data of these two proxies whenever possible. For the paleosol proxy, the greatest source of uncertainty is in the estimation of paleo-soil CO_2 concentration derived from respiration. Two different approaches are commonly used to estimate paleo-soil CO_2 concentration. The first method is based on proxy-estimated mean annual rainfall, whereas the second is based on soil order (i.e., the most general hierarchical level in soil taxonomy, comparable to kingdom in the classification of biological organisms). However, few records in the database allow for a direct comparison between the two approaches. An opportunity for comparison exists with two Eocene records (*37*, *42*), where recalculation using each of the two different methods leads to CO_2 estimates that do not overlap within 95% CIs for most stratigraphic levels (fig. S6). This implies that the uncertainty in estimating paleo-soil CO_2 concentration derived from respiration cannot be fully quantified with either of these approaches. Thus, most paleosol-based CO_2 estimates were designated as Category 2. For the phytoplankton proxy, routinely applied methods differ in how algal cell size and growth rate are accounted for, as well as the assumed sensitivity of algal $\delta^{13}C$ values to aqueous CO_2 concentration (see supplementary materials for details). Where data were available, we compared both newer and traditional methods, finding that although there are deviations between the resulting CO_2 estimates, they do agree within 95% CIs. We hence assign many phytoplankton CO_2 estimates to Category 1 and present mean CO_2 and uncertainty values that reflect the range of results from the different methods.

Toward a Cenozoic history of atmospheric CO_2

Our composite Category 1 and 2 realizations of Cenozoic CO_2 (Fig. 1, A and B) display much better agreement among proxies than does the raw, uncurated collection ("Archive," Fig. 1C). Encouragingly, objective criteria applied to the original data products automatically placed the earlier-reported estimates of "negative" CO_2, as well as some unusually high values, into Category 3, and without subjective intervention to otherwise filter them. We note that the Category 1 composite is now largely dominated by marine proxy estimates, with some intervals (e.g., the middle Paleocene, ~63 to

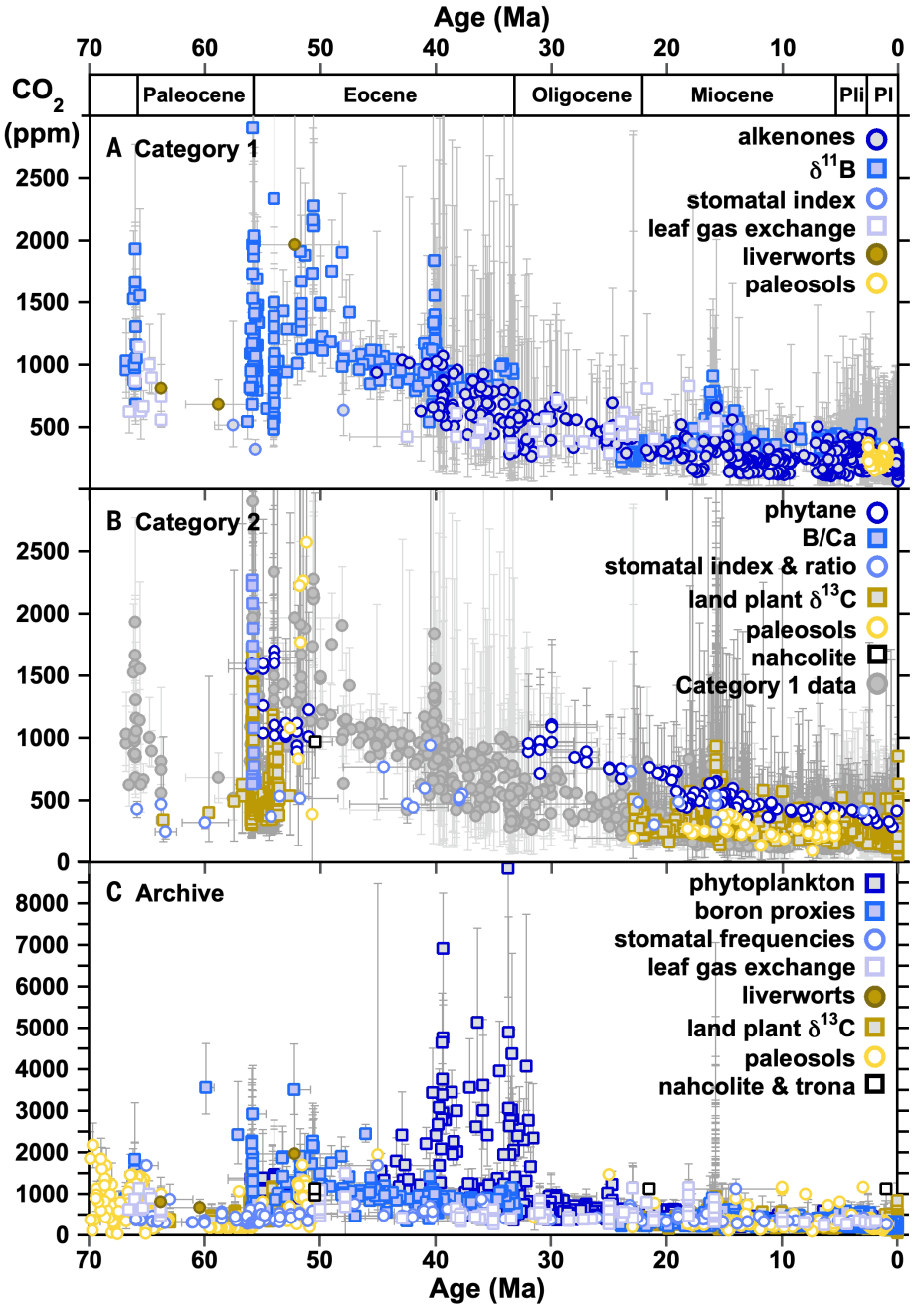

Fig. 1. Documentation and assessment of all Cenozoic paleo-CO_2 estimates published to date. Individual proxy estimates, as defined by the colored symbols in the legends. (**A**) Vetted Category 1 estimates with their fully developed uncertainty estimates (95% CIs); age uncertainties have been updated or established to the best of current understanding. (**B**) Vetted Category 2 estimates whose uncertainty is not yet fully constrained. Category 1 data are shown in gray for reference. (**C**) Archive compilation of all CO_2 estimates in their originally published quantification. To toggle view of individual proxy records in (A) and (C), please go to https://paleo-co2.org/. Pli, Pliocene; Pl, Pleistocene.

57 Ma) very sparsely sampled. Furthermore, some intervals (e.g., Oligocene, Miocene) still exhibit notable differences between proxies; for instance, marine-based CO_2 estimates start high and decline during the Oligocene (~34 to 23 Ma), whereas plant-based estimates suggest overall lower and constant CO_2 (Fig. 1A). Estimates of global temperature (Fig. 2B) during this time interval are largely invariant, which leaves us with the question of whether CO_2 and climate were decoupled during this interval, or whether there is a systematic bias in the marine or plant-based CO_2 proxies and/or in the temperature proxies. All proxy-based estimates become more uncertain further back in time as our knowledge of vital effects in biological proxy carriers, secular changes in the elemental and isotopic composition of ocean and atmosphere, and proxy sensitivity to environmental parameters that change along with CO_2 (e.g., temperature, rainfall; see supplementary materials for details) becomes less certain. In some cases, ancillary constraints and uncertainties are shared across multiple proxies (e.g., assumed atmospheric $\delta^{13}C$ is common to proxies based on land plant $\delta^{13}C$, leaf gas exchange, and paleosols), creating interdependence of estimates from seemingly independent proxies. More robust paleo-CO_2 reconstruction thus requires not only continued application of all proxies but also replication from different locations.

Although some uncertainties and proxy disagreements remain, the much-improved agreement within the vetted paleo-CO_2 compilation gives us confidence that a quantitative reconstruction of Cenozoic CO_2 based on the combined Category 1 data is possible. To do so, we statistically model mean CO_2 values at 500-kyr intervals, together with uncertainties in age and proxy CO_2 estimates (Fig. 2A; see supplementary materials for details). Our choice of a 500-kyr resolution interval reflects a compromise driven by the proxy data compilation. Although parts of the Cenozoic, particularly the Plio-Pleistocene, are sampled at higher temporal resolution, the density of records remains relatively sparse throughout much of the Paleogene (1 datum per 190 kyr on average). As a result, the data (and in some cases the underlying age models) are not suited to interpreting higher-frequency (e.g., Milankovitch-scale) variations in atmospheric composition, and we focus here on low-frequency (e.g., multimillion year) trends and transitions. Proxy sampling within some intervals may be biased toward conditions that deviate from the 500-kyr mean [most notably here, the Paleocene-Eocene Thermal Maximum (PETM)]. We do not attempt to remove this bias but instead recommend caution in interpreting any features expressed at submillion-year timescales.

This curve (Fig. 2A) allows us to constrain Cenozoic paleo-CO_2 and its uncertainty with greater confidence than earlier efforts. The highest CO_2 values of the past 66 Myr appear during the Early Eocene Climatic Optimum (EECO; ~53 to 51 Ma), whereas the lowest values occur during the Pleistocene. In contrast to earlier compilations, which suggested early Cenozoic CO_2 concentrations of <400 ppm (*33*), rigorous data vetting and newly published records place early Paleocene mean CO_2 in our reconstruction between 650 and 850 ppm. However, the Paleocene remains data-poor, and uncertainty in the curve remains large. Although the Paleocene record is predominantly based on the boron isotope proxy (Fig. 1A), inclusion of other (nonmarine) proxy data does

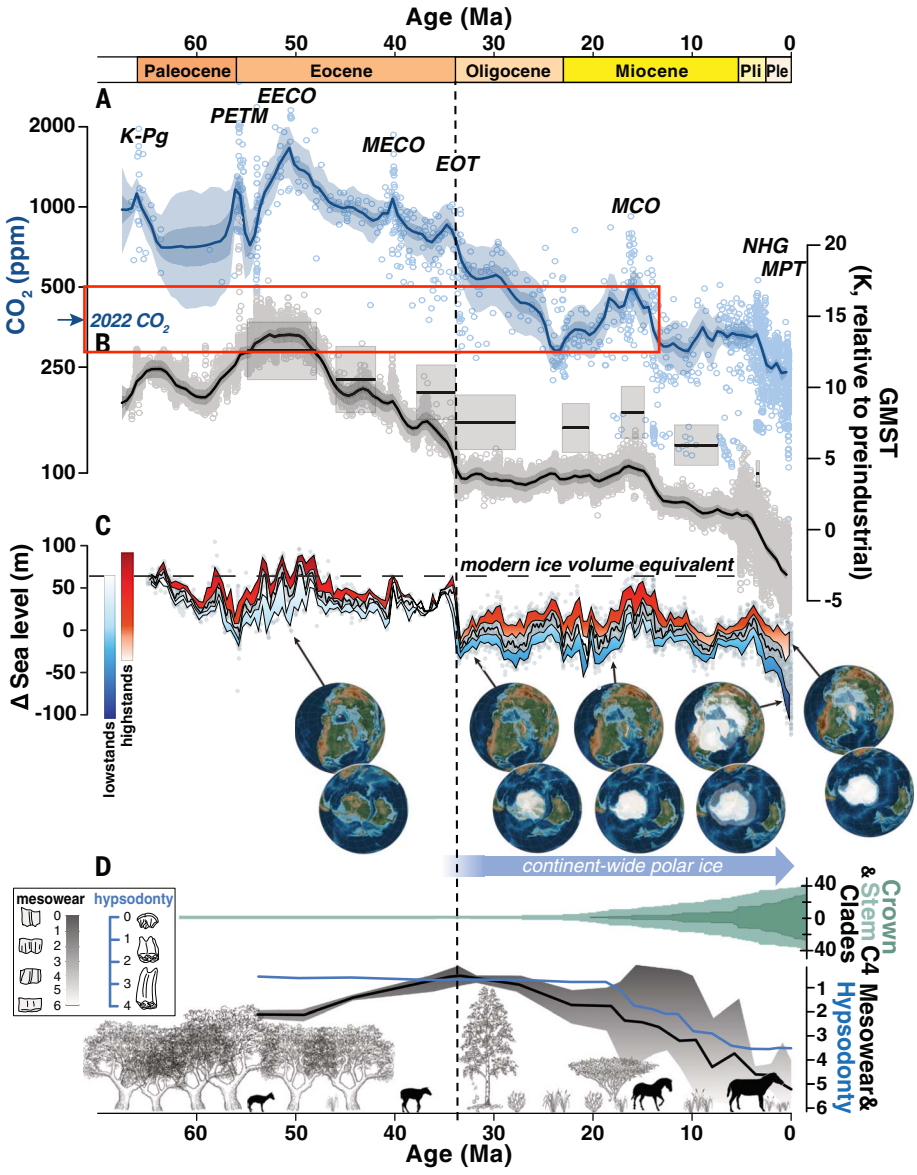

Fig. 2. Category 1 paleo-CO_2 record compared to global climate signals. The vertical dashed line indicates the onset of continent-wide glaciation in Antarctica. (**A**) Atmospheric CO_2 estimates (symbols) and 500-kyr mean statistical reconstructions (median and 50 and 95% credible intervals: dark and light-blue shading, respectively). Major climate events are highlighted: K-PG, Cretaceous/Paleogene boundary; PETM, Paleocene Eocene Thermal Maximum; EECO, Early Eocene Climatic Optimum; MECO, Middle Eocene Climatic Optimum; EOT, Eocene/Oligocene Transition; MCO, Miocene Climatic Optimum; NHG, onset of Northern Hemisphere Glaciation; and MPT, Mid-Pleistocene Transition. The 2022 annual average atmospheric CO_2 of 419 ppm is indicated for reference. (**B**) Global mean surface temperatures estimated from benthic $\delta^{18}O$ data following Westerhold *et al*. (*43*) (solid line, individual proxy estimates as symbols, and statistically reconstructed 500-kyr mean values shown as the continuous curve, with 50 and 95% credible intervals) and from surface temperature proxies (gray boxes) (*45*). (**C**) Sea level after (*66*) with gray dots displaying raw data; the solid black line reflects median sea level in a 1-Myr running window. High- and lowstands are defined within a running 400-kyr window, with lower and upper bounds of highstands defined by the 75th and 95th percentiles, and lower and upper bounds of lowstands defined by the 5th and 25th percentiles in each window. Globes depict select paleogeographic reconstructions and the growing presence of ice sheets in polar latitudes from (*116*). (**D**) Crown ages show that C_4 clades, with CCMs adapted to low CO_2, initially diversified in the early Miocene, and then rapidly radiated in the late Miocene (*117*). Flora transition from dominantly forested and woodland to open grassland habitats based on fossil phytolith abundance data (*96*). North American equids typify hoofed animal adaptations to new diet and environment (*103*), including increasing tooth mesowear (black line; note the inverted scale), hypsodonty (blue line), and body size.

influence and refine the reconstruction through this epoch, supporting the value of the multi-proxy approach (fig. S10). After the rapid CO_2 rise and fall associated with the PETM at 56 Ma, mean CO_2 steadily rose to peak values of ~1600 ppm around 51 Ma during the EECO. The middle and late Eocene recorded slightly lower values (800 to 1100 ppm). Mean CO_2 dropped to <600 ppm across the Eocene-Oligocene transition (EOT; 33.9 Ma) and reached values that generally fall between ~400 and 200 ppm during the Miocene through Pleistocene, except for a notable increase during the Middle Miocene (~17 to 15 Ma) to a mean of ~500 ppm. Uncertainty in the mean CO_2 values drops substantially in the Plio-Pleistocene (fig. S11), as expected given a drastic increase in data density. Our analysis suggests that ~14.5 to 14 Ma was the last time the 500-kyr–mean CO_2 value was as high as it is at present (fig. S11) and that all Plio-Pleistocene peak interglacial CO_2 concentrations were exceptionally likely to be less than those of the modern atmosphere (fig. S12). In contrast, before the Miocene, there is very little support (<2.5% probability) for Cenozoic 500-kyr–mean CO_2 values reaching or falling below preindustrial levels.

Climatic implications of the revised CO_2 curve

Relationship with global temperature change and climate sensitivity

Our reconstructed Cenozoic CO_2 trends are broadly coherent with those for global temperature as inferred, for instance, from the oxygen isotopic composition ($\delta^{18}O$) of fossil benthic foraminifera shells (*43*, *44*) and compilations of global surface temperature (*45*) (Fig. 2B). The Paleocene and Eocene epochs display overall higher temperatures and atmospheric CO_2 concentrations as compared with the later Oligocene, Miocene, and Pliocene—consistent with a predominantly greenhouse gas–regulated global energy budget. More specifically, the slow rise and subsequent fall of CO_2 over the course of the Paleocene and Eocene are mirrored by global temperatures, just as a transient Miocene CO_2 rise coincides with a period of warming at the Miocene Climatic Optimum (MCO). The EOT is identifiable in both the CO_2 and temperature records, despite the smoothing introduced by the curve fitting and 500-kyr binning interval.

Despite this overall agreement, rates and timing of CO_2 are not always synchronized with temperature changes in the two records (Fig. 2, A and B). For example, CO_2 appears broadly static or even rising during the late Eocene (37 to 34 Ma) and late Miocene (11 to 5 Ma) despite global cooling at these times (*46*). Conversely, decreasing CO_2 during the early Oligocene corresponds with relatively stable global temperatures [Fig. 2B, but see also (*47*, *48*)] and ice volume (Fig. 2C) at that time.

We note that the reconstructed Oligocene CO_2 decrease is driven by the contribution of marine proxies to the composite curve, whereas estimates from leaf gas exchange proxies are low and broadly static (Fig. 1C), a discrepancy that cannot be resolved without further experimentation and data collection. We caution that, even at the 500-kyr resolution of our study, the relative timing of CO_2 and temperature change might be unresolved in poorly sampled intervals (i.e., middle Paleocene) but should be well resolved during more-recent, well-sampled intervals (i.e., late Miocene through present; fig. S8). Is the occasional divergence of temperature and CO_2 change evidence for occasional disconnects between CO_2 forcing and climate response? Although one might posit bias in the CO_2 reconstruction, the strength of our multiproxy approach is the reduced likelihood that multiple proxies exhibit common bias during particular periods of the Cenozoic. We suggest that some cases of divergence between temperature and CO_2 could reflect non-CO_2 effects on climate [e.g., changes in paleogeography affecting ocean circulation, albedo, and heat transport (*49*)], or the temperature reconstructions used herein could be biased by nonthermal influences [e.g., uncertain elemental and isotopic composition of paleoseawater, physiological or pH effects on proxies (*48*, *50*)].

Our updated CO_2 curve, in conjunction with existing global temperature reconstructions, gives us the opportunity to reassess how climate sensitivity might have evolved through the Cenozoic. The most commonly reported form of climate sensitivity is equilibrium climate sensitivity (ECS), which focuses on fast feedback processes (e.g., clouds, lapse rate, snow, sea ice) and is therefore best suited for predicting present-day warming [~3°C for a doubling of CO_2 above the preindustrial condition (*2*)]. Because the average temporal resolution of our CO_2 database is coarser than 1000 years, we cannot estimate ECS directly. Instead, our data are most appropriate for interpreting an Earth system sensitivity [$ESS_{[CO2]}$, following the taxonomy of (*51*)]—the combination of short-term climate responses to doubling CO_2 plus the effects of slower, geological feedback loops such as the growth and decay of continental ice sheets. We compare our reconstructed 500-kyr–mean CO_2 values with two different estimates of global surface temperature. We apply the same Bayesian inversion model used in the CO_2 reconstruction to derive 500-kyr–mean surface temperatures from the benthic foraminiferal $\delta^{18}O$ compilation of (*43*), which we convert to temperatures using the methodology of (*44*) (Fig. 2B). In addition, we pair a set of multiproxy global surface temperature estimates for eight Cenozoic time intervals (Fig. 2B) (*45*) with posterior CO_2 estimates from time bins corresponding to each interval. The two temperature reconstructions are broadly similar, although the benthic record suggests relatively higher temperatures during the hothouse climate of the Paleocene and Eocene, whereas the multiproxy reconstruction is elevated relative to the benthic record during the Oligocene and Neogene.

The coevolution of atmospheric CO_2 and global mean surface temperature (GMST) over the Cenozoic is shown in Fig. 3. Because CO_2 is on a log scale, the slopes of lines connecting two adjacent points in time reflect the average intervening $ESS_{[CO2]}$. Benthic $\delta^{18}O$–derived temperatures suggest that early Paleocene warming occurs with a very high $ESS_{[CO2]}$ (>8°C per CO_2 doubling), although CO_2 uncertainties are large during this time interval. $ESS_{[CO2]}$ steadily declines toward the peak of Cenozoic warmth at ~50 Ma, then steepens again to ~8°C per CO_2 doubling for much of the cooling through to the EOT at ~34 Ma. In contrast, the multiproxy global temperature record suggests a lower $ESS_{[CO2]}$ of ~5°C between the early Eocene and earliest Oligocene. During the Oligocene and early part of the Miocene, both temperature records imply a near-zero $ESS_{[CO2]}$,

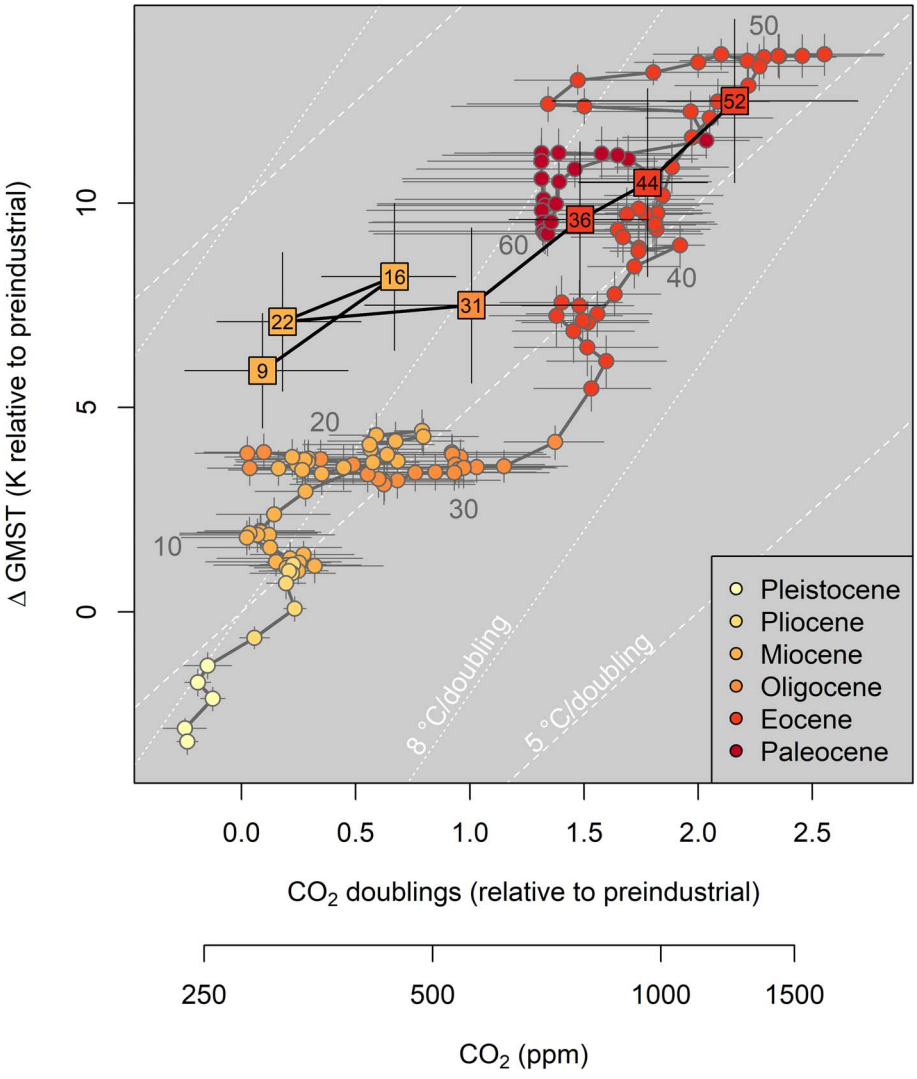

Fig. 3. Application of the Category 1 CO_2 record to determine $ESS_{[CO2]}$. GMST deviation (kelvin) from preindustrial global average surface temperature of 14.15°C is displayed versus paleo-CO_2 doublings relative to the preindustrial baseline of 280 ppm (upper *x* axis) and paleo-CO_2 estimates on a log scale (lower *x* axis). The slopes between two points in time reflect the average $ESS_{[CO2]}$. Circles reflect 500-kyr binned Category 1 CO_2 estimates paired with corresponding GMST means from (*43*); squares pair CO_2 and GMST means from compilations of sea surface temperature (*45*) in seven coarsely resolved time intervals. Note that this figure omits the Pliocene temperature estimate of (*45*) because it samples too short a time interval (compare with Fig. 2) to be comparable with mean CO_2. Data from Cenozoic epochs are color coded and shift from red (Paleocene) to yellow (Pleistocene); labels indicate specific age bins (Ma). Dashed lines indicate reference $ESS_{[CO2]}$ lines of 8° and 5°C warming per doubling of CO_2.

meaning that CO_2 values appear to decline with no appreciable global cooling. $ESS_{[CO2]}$ implied by both temperature reconstructions steepens again from the middle Miocene (~16 Ma) to present, averaging 8°C per CO_2 doubling over the past 10 Myr.

An alternative perspective on early Cenozoic climate forcing was introduced by (*44*), who hypothesized that all pre-Oligocene climate change was the response of direct and indirect CO_2 radiative forcing plus long-term change in solar output (i.e., constant albedo). Consequently, they converted Paleocene and Eocene benthic $\delta^{18}O$–derived GMST to estimates of CO_2 change required to explain the temperature record. Our reconstruction offers a direct test of this hypothesis, and although it compares well with the $\delta^{18}O$ approach of (*44*) throughout much of the early Cenozoic, our curve suggests that the late Eocene decline in CO_2 was less severe than expected under the constant albedo assumption (fig. S13). This result is consistent with a growing contribution of glacier and sea ice albedo effects (*52*, *53*) and the opening of Southern Ocean gateways (*54*) to climate cooling preceding the Eocene-Oligocene boundary.

In summary, the Cenozoic compilation confirms a strong link between CO_2 and GMST across timescales from 500 kyr to tens of millions of years, with $ESS_{[CO2]}$ generally within the range of 5° to 8°C—patterns consistent with most prior work (*32*–*34*, *45*, *51*, *55*–*60*) and considerably higher than the present-day ECS of ~3°C. Both temperature reconstructions imply relatively high $ESS_{[CO2]}$ values during the last 10 Myr of the Cenozoic, when global ice volumes were highest. This agrees with expectations of an amplified $ESS_{[CO2]}$ due to the ice-albedo feedback (*61*). However, even during times with little to no ice (Paleocene to early Eocene), we find elevated values of $ESS_{[CO2]}$ (approaching or exceeding 5°C per CO_2 doubling). This implies that fast, non-ice feedbacks, such as clouds or non-CO_2 greenhouse gases (*60*, *62*–*65*), were probably stronger in the early Paleogene than they are in the present-day climate system (*5*). The Oligocene to early Miocene is the most enigmatic interval, with an apparent decrease in CO_2 despite relatively stable temperature, implying near-zero $ESS_{[CO2]}$. It should be noted that this is one interval where different CO_2 proxies disagree on CO_2 change (Fig. 1A), with relatively stable values from plants but a decline in values from alkenones. More work is needed to confirm these CO_2 and temperature findings, but if these estimates are correct, this could partly reflect transition from a climate state too cold to support the strong, fast feedbacks (e.g., clouds) of the early Eocene (*5*) but not cold enough to generate strong ice-albedo feedback. Tectonic changes in the arrangement of continents and the opening of critical ocean gateways may also be confounding derivation of $ESS_{[CO2]}$ at that time (*49*, *54*).

Relationship with the evolution of the cryosphere

Our composite CO_2 record also enables reexamination of the evolution of Earth's cryosphere (Fig. 2C) in relation to CO_2 radiative forcing. We use the sea level estimation of (*66*) for this comparison because it covers the entire Cenozoic and is somewhat independent of the benthic $\delta^{18}O$ stack (*43*) used for the GMST derivation in Fig. 2B and also of the more recent sea level reconstruction of (*67*). Although there are substantial differences between the two sea level estimates, the main features discussed herein are broadly consistent between them. The establishment of a permanent, continent-wide Antarctic ice shield at the EOT (~34 Ma) comes at the end of a ~10-Myr period of generally slowly decreasing CO_2. There is evidence for isolated, unstable Antarctic glaciers at various points during the 10-Myr interval preceding the EOT (*50*, *53*, *66*, *68*), which is consistent with the increasing paleogeographic isolation of Antarctica and Southern Ocean cooling (*54*), and CO_2 may have been sufficiently low to enable the repeated crossing of a glaciation threshold by periodic orbital forcing. Tectonic cooling of Antarctica would have progressively raised the CO_2 glaciation threshold, which has been modeled to be between 560 and 920 ppm (*69*, *70*). Our composite CO_2 record allows us to further assess this glaciation threshold but requires determining the point during glacial inception when strong positive feedbacks (e.g., ice-albedo and ice sheet elevation) commenced and ice sheet growth accelerated (*71*). Using the sea level curve of (*66*), we determine this point to be 33.75 ±0.25 Ma, where our composite CO_2 record suggests 719^{+180}_{-152} ppm (95% CIs). Once established, the land-based Antarctic ice sheet likely persisted for the remainder of the Cenozoic, although substantial retreat of land-based ice has been modeled (30 to 36 m sea level equivalent) (*72*) and estimated from proxies (Fig. 2C) for the MCO. During the MCO, 500-kyr–mean CO_2 values increased to ~500 ppm (Fig. 2A and fig. S10), and benthic foraminiferal $\delta^{18}O$ (Fig. 2B) (*43*) and clumped isotopes (*50*) indicate warming. Although the stability of the land-based Antarctic ice sheet depends on many factors in addition to CO_2-induced global warming [e.g., hysteresis (*73*) and bed topography (*74*)], our composite record indicates that considerable retreat of land-based ice did not occur below 441 to 480 ppm (2.5th to 50th percentiles), and some land-based ice may have persisted up to 563 ppm (97.5th percentile) during the MCO. Excepting the MCO, atmospheric CO_2 has remained below our current value of 419 ppm since the late Oligocene (Fig. 2A and fig. S10), with relatively small sea level variations [up to ~20 m; Fig. 2C and (*67*)] being driven by orbitally forced melting of the marine-based ice sheet (*72*, *75*). Finally, at ~2.7 Ma, the transition to intensified Northern Hemisphere glaciation and orbitally driven glacial cycles coincided with CO_2 values that began decreasing after a relative high during the Pliocene (Fig. 2A).

Evolutionary implications of the revised CO_2 curve

Whereas geologic trends in terrestrial floral and faunal habitat ranges (*76*, *77*) and diversity (*78*–*80*) are largely thought to be controlled by temperature and associated climate patterns, atmospheric CO_2 has been hypothesized to drive the evolution of biological carbon-concentrating mechanisms (CCMs) and their subsequent diversification in terrestrial plants (Fig. 2D) (*81*, *82*). Our realization of how atmospheric CO_2 has varied through the Cenozoic allows us to reexamine this hypothesis. The two primary CCMs in terrestrial plants are the crassulacean acid metabolism (CAM) and C_4 photosynthetic syndromes. CCMs in terrestrial C_4 and CAM plants confer competitive advantages over the ancestral C_3 pathway under higher growing season temperatures, low rainfall, and lower atmospheric CO_2. As a result, C_4 photosynthesis contributes about 23% of today's global terrestrial gross primary production (*83*).

Plant clades with the C_4 pathway first emerged in the early Oligocene (*84*, *85*), yet they did not expand to ecological significance until the late Miocene [i.e., they contributed <5% of gross primary production before ~10 Ma; Fig. 2D and (*86*–*88*)]. CAM plants (e.g., cacti, ice plants, agaves, and some orchids) underwent substantial diversification events around the late Oligocene and late Miocene (*89*–*91*). Taken together, two general biological thresholds emerge from our CO_2 record: (i) All known origins of C_4 plants occurred when atmospheric CO_2 was lower than ~550 ppm [i.e., after 32 Ma; Fig. 2, A and D, and (*84*)], which is in agreement with theoretical predictions (*92*, *93*). (ii) All major Cenozoic CAM diversification events coincided with intervals when CO_2 was lower than ~430 ppm (i.e., after 27 Ma) (*89*, *90*). Our record is thus consistent with decreasing atmospheric CO_2 (<550 ppm) being a critical threshold for the Cenozoic origin, diversification, and expansion of C_4 and CAM plants within grasslands, arid habitats (such as deserts), and habits (such as epiphytes), and provides strong data support for previous hypotheses (*20*, *84*, *86*, *88*, *89*, *92*, *94*, *95*). Notably, after their origin in the early Oligocene, C_4 plants did not immediately proliferate. By ~24 to ~18 Ma, open habitat grasslands are evident on most continents (*96*), yet widespread dispersal of C_4 plants was delayed until the late Miocene and without any apparent decline in CO_2 (Fig. 2D). Therefore, the rise of C_4 plants to their dominance in many tropical and subtropical ecosystems was likely driven (and is maintained today) by other factors,

such as fire, seasonality of rainfall, and herbivory (i.e., grazing that keeps landscapes open) (*97*, *98*). The temporal evolution of these factors warrants further study as we move toward a future where CO_2 may rise above the 550-ppm threshold that was key to the origin, taxonomic diversification, and spread of C_4 plants.

Terrestrial mammals evolved and adapted to the changing and more-open floral ecosystems of the late Cenozoic (*99*–*101*) and are thus indirectly linked to the 550-ppm atmospheric CO_2 threshold discovered herein. In particular, dental wear patterns (such as the shape of the chewing surface of a tooth, i.e., mesowear) and tooth morphology, such as crown height, reflect an increasingly abrasive and tough diet (*102*, *103*) and can be traced across many herbivore lineages during this period. For instance, mesowear in North American Equidae (horses and their ancestors) (Fig. 2D) began to increase in the late Eocene and steadily continued to increase into the Quaternary. Similarly, equids evolved high-crowned (hypsodont) teeth in the Miocene (*103*–*105*), and their body size increased to accommodate higher intake of more-abrasive, grassy vegetation (Fig. 2D).

Evolutionary trends are a little less clear in the ocean, because marine algal CCMs are ubiquitous and diverse in form (*106*) and are believed to have an ancient origin. Moreover, the large spatial and seasonal variance of dissolved CO_2 in the surface ocean (as compared with the relatively uniform seasonal and spatial concentration of CO_2 in the air) may somewhat decouple their evolution from geologic trends in atmospheric CO_2. Evidence exists that marine algae, and in particular the coccolithophores (i.e., the source of the alkenone biomarkers), express CCMs to a greater extent when CO_2 is lower (*107*–*109*), with estimates of cellular carbon fluxes suggesting that enhanced CCM activity in coccolithophores began between ~7 and 5 Ma (*110*). However, our revised CO_2 curve displays mean atmospheric CO_2 broadly constant at 300 to 350 ppm since at least ~14 Ma (Fig. 2A and fig. S10), suggesting that increased CCM activity may reflect other proximal triggers, perhaps involving changes in ocean circulation and nutrient supply.

Perspectives and opportunities for further advances

Our community-assessed composite CO_2 record and statistically modeled time-averaged CO_2 curve exhibit greater clarity in the Cenozoic evolution of CO_2 and its relationship with climate than was possible in previous compilations and furthermore highlight the value of cross-disciplinary collaboration and community building. Generating a paleo-CO_2 record with even greater confidence requires targeted efforts using multiple proxies to fill in data gaps, higher resolution and replication from multiple locations, and novel approaches to resolve remaining differences between CO_2 proxy estimates. Specifically, although the number and diversity of paleo-CO_2 proxy records continue to grow, data remain relatively sparse during several key parts of the Cenozoic record (e.g., middle Paleocene, Oligocene). Moreover, records from the Paleocene and Eocene are dominated by estimates from the boron isotope proxy, increasing the potential for bias. Targeted efforts are hence needed to expand the number and diversity of data through these intervals and to refine multiproxy reconstructions. Additionally, despite substantial progress, there remains a lack of consensus regarding the identity and/or quantification of some of the factors underlying each of the proxy systems analyzed here. New experimental and calibration studies, particularly those that isolate and quantify specific mechanistic responses and/or their interactions, need to be undertaken to reduce potential biases and uncertainty for each method. For instance, the emerging fields of genomics, evolutionary and developmental biology, and proteomics provide exciting opportunities for improving and understanding paleoproxy systematics. Furthermore, and associated with improved experimental quantification, refining our theoretical and mechanistic understanding of how proxies are encoded will allow us to create explicit and self-consistent representations of the processes involved. The development of proxy system forward models provides a promising leap in this direction (*111*). Bayesian statistical methods can then enable the full suite of models and data to be integrated and constrain the range of environmental conditions, including atmospheric CO_2 and other variables that are consistent with the multiproxy data (*112*, *113*). Finally, development of new proxies is also a realistic and desirable aim. For instance, while this study focuses on more established proxies, new proxies such as coccolith calcite stable isotopes (*114*) and mammalian bone and teeth oxygen-17 anomalies (*115*) show promising results for reconstructing paleo-CO_2 but perhaps require further validation before they can be assessed with confidence.

Proxies and proxy-based reconstructions of how atmospheric CO_2 has varied through deep time have improved immeasurably over the past few decades. Although they will never allow us to reconstruct past CO_2 with the same fidelity as direct air measurement, our study shows how community-based consensus assessment, together with a critical reanalysis of proxy models and assumptions, can progressively move us toward a quantitative history of atmospheric CO_2 for geological time.

REFERENCES AND NOTES

1. S. Arrhenius, XXXI. On the influence of carbonic acid in the air upon the temperature of the ground. *Lond. Edinb. Dublin Philos. Mag. J. Sci.* **41**, 237–276 (1896). doi: 10.1080/14786449608620846
2. IPCC, *Climate Change 2021: The Physical Science Basis. Contribution of Working Group I to the Sixth Assessment Report of the Intergovernmental Panel on Climate Change*, V. Masson-Delmotte *et al.*, Eds. (Cambridge Univ. Press, 2021).
3. P. Tans, R. Keeling, "Carbon cycle greenhouse gases: Trends in atmospheric carbon dioxide" (National Oceanic and Atmospheric Administration, Earth System Research Laboratories, Global Monitoring Laboratory, 2023); www.esrl.noaa.gov/gmd/ccgg/trends/.
4. K. E. Taylor, R. J. Stouffer, G. A. Meehl, An overview of CMIP5 and the experiment design. *Bull. Am. Meteorol. Soc.* **93**, 485–498 (2011). doi: 10.1175/BAMS-D-11-00094.1
5. R. Caballero, M. Huber, State-dependent climate sensitivity in past warm climates and its implications for future climate projections. *Proc. Natl. Acad. Sci. U.S.A.* **110**, 14162–14167 (2013). doi: 10.1073/pnas.1303365110; pmid: 23918397
6. J. Zhu, C. J. Poulsen, On the increase of climate sensitivity and cloud feedback with warming in the community atmosphere models. *Geophys. Res. Lett.* **47**, e2020GL089143 (2020). doi: 10.1029/2020GL089143
7. J. Zhu, C. J. Poulsen, B. L. Otto-Bliesner, High climate sensitivity in CMIP6 model not supported by paleoclimate. *Nat. Clim. Chang.* **10**, 378–379 (2020). doi: 10.1038/s41558-020-0764-6
8. E. J. Judd *et al.*, The PhanSST global database of Phanerozoic sea surface temperature proxy data. *Sci. Data* **9**, 753 (2022). doi: 10.1038/s41597-022-01826-0; pmid: 36473868
9. R. J. Delmas, J.-M. Ascencio, M. Legrand, Polar ice evidence that atmospheric CO_2 20,000 yr BP was 50% of present. *Nature* **284**, 155–157 (1980). doi: 10.1038/284155a0
10. A. Neftel, H. Oeschger, J. Schwander, B. Stauffer, R. Zumbrunn, Ice core sample measurements give atmospheric CO_2 content during the past 40,000 yr. *Nature* **295**, 220–223 (1982). doi: 10.1038/295220a0
11. B. Bereiter *et al.*, Revision of the EPICA Dome C CO_2 record from 800 to 600 kyr before present. *Geophys. Res. Lett.* **42**, 542–549 (2015). doi: 10.1002/2014GL061957
12. Y. Yan *et al.*, Two-million-year-old snapshots of atmospheric gases from Antarctic ice. *Nature* **574**, 663–666 (2019). doi: 10.1038/s41586-019-1692-3; pmid: 31666720
13. J. A. Higgins *et al.*, Atmospheric composition 1 million years ago from blue ice in the Allan Hills, Antarctica. *Proc. Natl. Acad. Sci. U.S.A.* **112**, 6887–6891 (2015). doi: 10.1073/pnas.1420232112; pmid: 25964367
14. C. Nehrbass-Ahles *et al.*, Abrupt CO_2 release to the atmosphere under glacial and early interglacial climate conditions. *Science* **369**, 1000–1005 (2020). doi: 10.1126/science.aay8178; pmid: 32820127
15. C. Le Quéré *et al.*, Trends in the sources and sinks of carbon dioxide. *Nat. Geosci.* **2**, 831–836 (2009). doi: 10.1038/ngeo689
16. P. Friedlingstein *et al.*, Global carbon budget 2022. *Earth Syst. Sci. Data* **14**, 4811–4900 (2022). doi: 10.5194/essd-14-4811-2022
17. P. Valdes, Built for stability. *Nat. Geosci.* **4**, 414–416 (2011). doi: 10.1038/ngeo1200
18. W. Kiessling, M. Aberhan, L. Villier, Phanerozoic trends in skeletal mineralogy driven by mass extinctions. *Nat. Geosci.* **1**, 527–530 (2008). doi: 10.1038/ngeo251
19. J. L. Payne, A. M. Bush, N. A. Heim, M. L. Knope, D. J. McCauley, Ecological selectivity of the emerging mass extinction in the oceans. *Science* **353**, 1284–1286 (2016). doi: 10.1126/science.aaf2416; pmid: 27629258
20. E. J. Edwards *et al.*, The origins of C_4 grasslands: Integrating evolutionary and ecosystem science. *Science* **328**, 587–591 (2010). doi: 10.1126/science.1177216; pmid: 20431008
21. F. A. McInerney, S. L. Wing, The Paleocene-Eocene Thermal Maximum: A perturbation of carbon cycle, climate, and biosphere with implications for the future. *Annu. Rev. Earth Planet. Sci.* **39**, 489–516 (2011). doi: 10.1146/annurev-earth-040610-133431
22. W. Konrad, D. L. Royer, P. J. Franks, A. Roth-Nebelsick, Quantitative critique of leaf-based paleo-CO_2 proxies: Consequences for their reliability and applicability. *Geol. J.* **56**, 886–902 (2020). doi: 10.1002/gj.3807
23. J. C. McElwain, M. Steinthorsdottir, Paleoecology, ploidy, paleoatmospheric composition, and developmental biology: A review of the multiple uses of fossil stomata. *Plant Physiol.* **174**, 650–664 (2017). doi: 10.1104/pp.17.00204; pmid: 28495890
24. B. A. Schubert, A. H. Jahren, The effect of atmospheric CO_2 concentration on carbon isotope fractionation in C_3 land plants. *Geochim. Cosmochim. Acta* **96**, 29–43 (2012). doi: 10.1016/j.gca.2012.08.003

25. T. E. Cerling, Carbon dioxide in the atmosphere; evidence from Cenozoic and Mesozoic Paleosols. *Am. J. Sci.* **291**, 377–400 (1991). doi: 10.2475/ajs.291.4.377
26. D. O. Breecker, Quantifying and understanding the uncertainty of atmospheric CO_2 concentrations determined from calcic paleosols. *Geochem. Geophys. Geosyst.* **14**, 3210–3220 (2013). doi: 10.1002/ggge.20189
27. E. A. Jagniecki, T. K. Lowenstein, D. M. Jenkins, R. V. Demicco, Eocene atmospheric CO_2 from the nahcolite proxy. *Geology* **43**, 1075–1078 (2015).
28. T. K. Lowenstein, R. V. Demicco, Elevated Eocene atmospheric CO_2 and its subsequent decline. *Science* **313**, 1928 (2006). doi: 10.1126/science.1129555; pmid: 17008525
29. M. Pagani, "12.13 - Biomarker-based inferences of past climate: The alkenone pCO_2 proxy" in *Treatise on Geochemistry*, vol. 12, H. D. Holland, K. K. Turekian, Eds. (Elsevier, ed. 2, 2014), pp. 361–378. doi: 10.1016/B978-0-08-095975-7.01027-5
30. B. Hönisch *et al*., *Boron Proxies in Paleoceanography and Paleoclimatology*, Analytical Methods in Earth and Environmental Science Series (John Wiley & Sons, Ltd., 2019).
31. J. W. B. Rae, "Boron isotopes in foraminifera: Systematics, biomineralisation, and CO_2 reconstruction" in *Boron Isotopes: The Fifth Element*, H. Marschall, G. Foster, Eds. (Springer International Publishing, 2018), pp. 107–143. doi: 10.1007/978-3-319-64666-4_5
32. D. J. Beerling, D. L. Royer, Convergent Cenozoic CO_2 history. *Nat. Geosci.* **4**, 418–420 (2011). doi: 10.1038/ngeo1186
33. G. L. Foster, D. L. Royer, D. J. Lunt, Future climate forcing potentially without precedent in the last 420 million years. *Nat. Commun.* **8**, 14845 (2017). doi: 10.1038/ncomms14845; pmid: 28375201
34. J. W. B. Rae *et al*., Atmospheric CO_2 over the past 66 million years from marine archives. *Annu. Rev. Earth Planet. Sci.* **49**, 609–641 (2021). doi: 10.1146/annurev-earth-082420-063026
35. S. Ji *et al*., A symmetrical CO_2 peak and asymmetrical climate change during the middle Miocene. *Earth Planet. Sci. Lett.* **499**, 134–144 (2018). doi: 10.1016/j.epsl.2018.07.011
36. J. Da, Y. G. Zhang, G. Li, X. Meng, J. Ji, Low CO_2 levels of the entire Pleistocene epoch. *Nat. Commun.* **10**, 4342 (2019). doi: 10.1038/s41467-019-12357-5; pmid: 31554805
37. E. Hyland, N. D. Sheldon, M. Fan, Terrestrial paleoenvironmental reconstructions indicate transient peak warming during the early Eocene climatic optimum. *Geol. Soc. Am. Bull.* **125**, 1338–1348 (2013). doi: 10.1130/B30761.1
38. J. Henderiks, M. Pagani, Refining ancient carbon dioxide estimates: Significance of coccolithophore cell size for alkenone-based pCO_2 records. *Paleoceanography* **22**, PA3202 (2007). doi: 10.1029/2006PA001399
39. S. R. Phelps *et al*., Carbon isotope fractionation in Noelaerhabdaceae algae in culture and a critical evaluation of the alkenone paleobarometer. *Geochem. Geophys. Geosyst.* **22**, e2021GC009657 (2021). doi: 10.1029/2021GC009657
40. H. M. Stoll *et al*., Upregulation of phytoplankton carbon concentrating mechanisms during low CO_2 glacial periods and implications for the phytoplankton pCO_2 proxy. *Quat. Sci. Rev.* **208**, 1–20 (2019). doi: 10.1016/j.quascirev.2019.01.012
41. Y. G. Zhang, J. Henderiks, X. Liu, Refining the alkenone-pCO2 method II: Towards resolving the physiological parameter 'b'. *Geochim. Cosmochim. Acta* **281**, 118–134 (2020). doi: 10.1016/j.gca.2020.05.002
42. E. G. Hyland, N. D. Sheldon, Coupled CO_2-climate response during the Early Eocene Climatic Optimum. *Palaeogeogr. Palaeoclimatol. Palaeoecol.* **369**, 125–135 (2013). doi: 10.1016/j.palaeo.2012.10.011
43. T. Westerhold *et al*., An astronomically dated record of Earth's climate and its predictability over the last 66 million years. *Science* **369**, 1383–1387 (2020). doi: 10.1126/science.aba6853; pmid: 32913105
44. J. Hansen, M. Sato, G. Russell, P. Kharecha, Climate sensitivity, sea level and atmospheric carbon dioxide. *Philos. Trans. A Math. Phys. Eng. Sci.* **371**, 20120294 (2013). doi: 10.1098/rsta.2012.0294; pmid: 24043864
45. S. J. Ring, S. G. Mutz, T. A. Ehlers, Cenozoic proxy constraints on earth system sensitivity to greenhouse gases. *Paleoceanogr. Paleoclimatol.* **37**, e2021PA004364 (2022). doi: 10.1029/2021PA004364
46. T. D. Herbert *et al*., Late Miocene global cooling and the rise of modern ecosystems. *Nat. Geosci.* **9**, 843–847 (2016). doi: 10.1038/ngeo2813
47. D. E. Gaskell *et al*., The latitudinal temperature gradient and its climate dependence as inferred from foraminiferal $\delta^{18}O$ over the past 95 million years. *Proc. Natl. Acad. Sci. U.S.A.* **119**, e2111332119 (2022). doi: 10.1073/pnas.2111332119; pmid: 35254906
48. C. L. O'Brien *et al*., The enigma of Oligocene climate and global surface temperature evolution. *Proc. Natl. Acad. Sci. U.S.A.* **117**, 25302–25309 (2020). doi: 10.1073/pnas.2003914117; pmid: 32989142
49. D. J. Lunt *et al*., Palaeogeographic controls on climate and proxy interpretation. *Clim. Past* **12**, 1181–1198 (2016). doi: 10.5194/cp-12-1181-2016
50. A. N. Meckler *et al*., Cenozoic evolution of deep ocean temperature from clumped isotope thermometry. *Science* **377**, 86–90 (2022). doi: 10.1126/science.abk0604; pmid: 35771913
51. PALAEOSENS Project Members, Making sense of palaeoclimate sensitivity. *Nature* **491**, 683–691 (2012). doi: 10.1038/nature11574; pmid: 23192145
52. A. Tripati, D. Darby, Evidence for ephemeral middle Eocene to early Oligocene Greenland glacial ice and pan-Arctic sea ice. *Nat. Commun.* **9**, 1038 (2018). doi: 10.1038/s41467-018-03180-5; pmid: 29531221
53. H. D. Scher, S. M. Bohaty, B. W. Smith, G. H. Munn, Isotopic interrogation of a suspected late Eocene glaciation. *Paleoceanography* **29**, 628–644 (2014). doi: 10.1002/2014PA002648
54. I. Sauermilch *et al*., Gateway-driven weakening of ocean gyres leads to Southern Ocean cooling. *Nat. Commun.* **12**, 6465 (2021). doi: 10.1038/s41467-021-26658-1; pmid: 34753912
55. D. L. Royer, Climate sensitivity in the geologic past. *Annu. Rev. Earth Planet. Sci.* **44**, 277–293 (2016). doi: 10.1146/annurev-earth-100815-024150
56. R. M. Brown, T. B. Chalk, A. J. Crocker, P. A. Wilson, G. L. Foster, Late Miocene cooling coupled to carbon dioxide with Pleistocene-like climate sensitivity. *Nat. Geosci.* **15**, 664–670 (2022). doi: 10.1038/s41561-022-00982-7
57. T. E. Wong, Y. Cui, D. L. Royer, K. Keller, A tighter constraint on Earth-system sensitivity from long-term temperature and carbon-cycle observations. *Nat. Commun.* **12**, 3173 (2021). doi: 10.1038/s41467-021-23543-9; pmid: 34039993
58. D. L. Royer, M. Pagani, D. J. Beerling, Geobiological constraints on Earth system sensitivity to CO_2 during the Cretaceous and Cenozoic. *Geobiology* **10**, 298–310 (2012). doi: 10.1111/j.1472-4669.2012.00320.x; pmid: 22353368
59. J. E. Tierney *et al*., Spatial patterns of climate change across the Paleocene-Eocene Thermal Maximum. *Proc. Natl. Acad. Sci. U.S.A.* **119**, e2205326119 (2022). doi: 10.1073/pnas.2205326119; pmid: 36215472
60. E. Anagnostou *et al*., Proxy evidence for state-dependence of climate sensitivity in the Eocene greenhouse. *Nat. Commun.* **11**, 4436 (2020). doi: 10.1038/s41467-020-17887-x; pmid: 32895377
61. J. Hansen *et al*., Target atmospheric CO: Where should humanity aim? *Open Atmos. Sci. J.* **2**, 217–231 (2008). doi: 10.2174/1874282300802010217
62. J. T. Kiehl, C. A. Shields, Sensitivity of the Palaeocene-Eocene Thermal Maximum climate to cloud properties. *Philos. Trans. A Math. Phys. Eng. Sci.* **371**, 20130093 (2013). doi: 10.1098/rsta.2013.0093; pmid: 24043867
63. J. Zhu, C. J. Poulsen, J. E. Tierney, Simulation of Eocene extreme warmth and high climate sensitivity through cloud feedbacks. *Sci. Adv.* **5**, eaax1874 (2019). doi: 10.1126/sciadv.aax1874; pmid: 31555736
64. D. J. Beerling, A. Fox, D. S. Stevenson, P. J. Valdes, Enhanced chemistry-climate feedbacks in past greenhouse worlds. *Proc. Natl. Acad. Sci. U.S.A.* **108**, 9770–9775 (2011). doi: 10.1073/pnas.1102409108; pmid: 21628580
65. T. Schneider, C. M. Kaul, K. G. Pressel, Possible climate transitions from breakup of stratocumulus decks under greenhouse warming. *Nat. Geosci.* **12**, 163–167 (2019). doi: 10.1038/s41561-019-0310-1
66. K. G. Miller *et al*., Cenozoic sea-level and cryospheric evolution from deep-sea geochemical and continental margin records. *Sci. Adv.* **6**, eaaz1346 (2020). doi: 10.1126/sciadv.aaz1346; pmid: 32440543
67. E. J. Rohling *et al*., Sea level and deep-sea temperature reconstructions suggest quasi-stable states and critical transitions over the past 40 million years. *Sci. Adv.* **7**, eabf5326 (2021). doi: 10.1126/sciadv.abf5326; pmid: 34172440
68. M. J. Henehan *et al*., Revisiting the Middle Eocene Climatic Optimum "carbon cycle conundrum" with new estimates of atmospheric pCO_2 from boron isotopes. *Paleoceanogr. Paleoclimatol.* **35**, e2019PA003713 (2020). doi: 10.1029/2019PA003713
69. E. Gasson *et al*., Uncertainties in the modelled CO_2 threshold for Antarctic glaciation. *Clim. Past* **10**, 451–466 (2014). doi: 10.5194/cp-10-451-2014
70. R. M. Deconto *et al*., Thresholds for Cenozoic bipolar glaciation. *Nature* **455**, 652–656 (2008). doi: 10.1038/nature07337; pmid: 18833277
71. R. M. DeConto, D. Pollard, Rapid Cenozoic glaciation of Antarctica induced by declining atmospheric CO_2. *Nature* **421**, 245–249 (2003). doi: 10.1038/nature01290; pmid: 12529638
72. E. Gasson, R. M. DeConto, D. Pollard, R. H. Levy, Dynamic Antarctic ice sheet during the early to mid-Miocene. *Proc. Natl. Acad. Sci. U.S.A.* **113**, 3459–3464 (2016). doi: 10.1073/pnas.1516130113; pmid: 26903645
73. D. Pollard, R. M. DeConto, Hysteresis in Cenozoic Antarctic ice-sheet variations. *Global Planet. Change* **45**, 9–21 (2005). doi: 10.1016/j.gloplacha.2004.09.011
74. G. J. G. Paxman, E. G. W. Gasson, S. S. R. Jamieson, M. J. Bentley, F. Ferraccioli, Long-term increase in Antarctic Ice Sheet vulnerability driven by bed topography evolution. *Geophys. Res. Lett.* **47**, e2020GL090003 (2020). doi: 10.1029/2020GL090003
75. J. J. Fürst *et al*., The safety band of Antarctic ice shelves. *Nat. Clim. Chang.* **6**, 479–482 (2016). doi: 10.1038/nclimate2912
76. J. C. McElwain, Paleobotany and global change: Important lessons for species to biomes from vegetation responses to past global change. *Annu. Rev. Plant Biol.* **69**, 761–787 (2018). doi: 10.1146/annurev-arplant-042817-040405; pmid: 29719166
77. S.-M. Popescu *et al*., Mangrove distribution and diversity during three Cenozoic thermal maxima in the Northern Hemisphere (pollen records from the Arctic–North Atlantic–Mediterranean regions). *J. Biogeogr.* **48**, 2771–2784 (2021). doi: 10.1111/jbi.14238
78. C. Jaramillo, M. J. Rueda, G. Mora, Cenozoic plant diversity in the neotropics. *Science* **311**, 1893–1896 (2006). doi: 10.1126/science.1121380; pmid: 16574860
79. J. Y. Lim *et al*., The Cenozoic history of palms: Global diversification, biogeography and the decline of megathermal forests. *Glob. Ecol. Biogeogr.* **31**, 425–439 (2022). doi: 10.1111/geb.13436
80. A. Graham, The age and diversification of terrestrial New World ecosystems through Cretaceous and Cenozoic time. *Am. J. Bot.* **98**, 336–351 (2011). doi: 10.3732/ajb.1000353; pmid: 21613130
81. J. R. Ehleringer, R. K. Monson, Evolutionary and ecological aspects of photosynthetic pathway variation. *Annu. Rev. Ecol. Syst.* **24**, 411–439 (1993). doi: 10.1146/annurev.es.24.110193.002211
82. H. Griffiths, "Carbon dioxide concentrating mechanisms and the evolution of CAM in vascular epiphytes" in *Vascular Plants as Epiphytes: Evolution and Ecophysiology*, U. Lüttge, Ed. (Springer, 1989), pp. 42–86. doi: 10.1007/978-3-642-74465-5_3
83. C. J. Still, J. A. Berry, G. J. Collatz, R. S. DeFries, Global distribution of C_3 and C_4 vegetation: Carbon cycle implications. *Global Biogeochem. Cycles* **17**, 1006 (2003). doi: 10.1029/2001GB001807
84. P.-A. Christin *et al*., Oligocene CO_2 decline promoted C_4 photosynthesis in grasses. *Curr. Biol.* **18**, 37–43 (2008). doi: 10.1016/j.cub.2007.11.058; pmid: 18160293
85. A. Vicentini, J. C. Barber, S. S. Aliscioni, L. M. Giussani, E. A. Kellogg, The age of the grasses and clusters of origins of C_4 photosynthesis. *Glob. Change Biol.* **14**, 2963–2977 (2008). doi: 10.1111/j.1365-2486.2008.01688.x
86. P. J. Polissar, C. Rose, K. T. Uno, S. R. Phelps, P. deMenocal, Synchronous rise of African C_4 ecosystems 10 million years ago in the absence of aridification. *Nat. Geosci.* **12**, 657–660 (2019). doi: 10.1038/s41561-019-0399-2
87. L. Tauxe, S. J. Feakins, A reassessment of the chronostratigraphy of late Miocene C_3–C_4 transitions. *Paleoceanogr. Paleoclimatol.* **35**, e2020PA003857 (2020). doi: 10.1029/2020PA003857
88. T. E. Cerling *et al*., Global vegetation change through the Miocene/Pliocene boundary. *Nature* **389**, 153–158 (1997). doi: 10.1038/38229
89. M. Arakaki *et al*., Contemporaneous and recent radiations of the world's major succulent plant lineages. *Proc. Natl. Acad.*

Sci. U.S.A. **108**, 8379–8384 (2011). doi: 10.1073/pnas.1100628108; pmid: 21536881
90. T. J. Givnish *et al*., Orchid phylogenomics and multiple drivers of their extraordinary diversification. *Proc. Biol. Sci.* **282**, 20151553 (2015). doi: 10.1098/rspb.2015.1553; pmid: 26311671
91. E. J. Edwards, Evolutionary trajectories, accessibility and other metaphors: The case of C_4 and CAM photosynthesis. *New Phytol.* **223**, 1742–1755 (2019). doi: 10.1111/nph.15851; pmid: 30993711
92. J. R. Ehleringer, T. E. Cerling, B. R. Helliker, C_4 photosynthesis, atmospheric CO_2, and climate. *Oecologia* **112**, 285–299 (1997). doi: 10.1007/s004420050311; pmid: 28307475
93. H. Zhou, B. R. Helliker, M. Huber, A. Dicks, E. Akçay, C_4 photosynthesis and climate through the lens of optimality. *Proc. Natl. Acad. Sci. U.S.A.* **115**, 12057–12062 (2018). doi: 10.1073/pnas.1718988115; pmid: 30401739
94. C. E. R. Lehmann, S. A. Archibald, W. A. Hoffmann, W. J. Bond, Deciphering the distribution of the savanna biome. *New Phytol.* **191**, 197–209 (2011). doi: 10.1111/j.1469-8137.2011.03689.x; pmid: 21463328
95. W. M. Kürschner, Z. Kvacek, D. L. Dilcher, The impact of Miocene atmospheric carbon dioxide fluctuations on climate and the evolution of terrestrial ecosystems. *Proc. Natl. Acad. Sci. U.S.A.* **105**, 449–453 (2008). doi: 10.1073/pnas.0708588105; pmid: 18174330
96. C. A. E. Strömberg, Evolution of grasses and grassland ecosystems. *Annu. Rev. Earth Planet. Sci.* **39**, 517–544 (2011). doi: 10.1146/annurev-earth-040809-152402
97. A. T. Karp, K. T. Uno, P. J. Polissar, K. H. Freeman, Late Miocene C_4 grassland fire feedbacks on the Indian subcontinent. *Paleoceanogr. Paleoclimatol.* **36**, e2020PA004106 (2021). doi: 10.1029/2020PA004106
98. T. Kukla *et al*., Drier winters drove Cenozoic open habitat expansion in North America. *AGU Adv.* **3**, e2021AV000566 (2022). doi: 10.1029/2021AV000566
99. M. Fortelius *et al*., Evolution of Neogene mammals in Eurasia: Environmental forcing and biotic interactions. *Annu. Rev. Earth Planet. Sci.* **42**, 579–604 (2014). doi: 10.1146/annurev-earth-050212-124030
100. F. Kaya *et al*., The rise and fall of the Old World savannah fauna and the origins of the African savannah biome. *Nat. Ecol. Evol.* **2**, 241–246 (2018). doi: 10.1038/s41559-017-0414-1; pmid: 29292396
101. C. M. Janis, J. Damuth, J. M. Theodor, Miocene ungulates and terrestrial primary productivity: Where have all the browsers gone? *Proc. Natl. Acad. Sci. U.S.A.* **97**, 7899–7904 (2000). doi: 10.1073/pnas.97.14.7899; pmid: 10884422
102. M. Fortelius, N. Solounias, Functional characterization of ungulate molars using the abrasion-attrition wear gradient: A new method for reconstructing paleodiets. *Am. Mus. Novit.* **3301**, 1–36 (2000). doi: 10.1206/0003-0082(2000)301<0001:FCOUMU>2.0.CO;2
103. M. C. Mihlbachler, F. Rivals, N. Solounias, G. M. Semprebon, Dietary change and evolution of horses in North America. *Science* **331**, 1178–1181 (2011). doi: 10.1126/science.1196166; pmid: 21385712
104. C. A. E. Strömberg, Evolution of hypsodonty in equids: Testing a hypothesis of adaptation. *Paleobiology* **32**, 236–258 (2006). doi: 10.1666/0094-8373(2006)32[236:EOHIET]2.0.CO;2
105. C. M. Janis, M. Fortelius, On the means whereby mammals achieve increased functional durability of their dentitions, with special reference to limiting factors. *Biol. Rev. Camb. Philos. Soc.* **63**, 197–230 (1988). doi: 10.1111/j.1469-185X.1988.tb00630.x; pmid: 3042033
106. M. R. Badger, D. Hanson, G. D. Price, Evolution and diversity of CO_2 concentrating mechanisms in cyanobacteria. *Funct. Plant Biol.* **29**, 161–173 (2002). doi: 10.1071/PP01213; pmid: 32689463
107. M. P. S. Badger, Alkenone isotopes show evidence of active carbon concentrating mechanisms in coccolithophores as aqueous carbon dioxide concentrations fall below 7 μmol L^{-1}. *Biogeosciences* **18**, 1149–1160 (2021). doi: 10.5194/bg-18-1149-2021
108. Y. G. Zhang, M. Pagani, Z. Liu, S. M. Bohaty, R. Deconto, A 40-million-year history of atmospheric CO_2. *Philos. Trans. A Math. Phys. Eng. Sci.* **371**, 20130096 (2013). doi: 10.1098/rsta.2013.0096; pmid: 24043869
109. P. D. Tortell, Evolutionary and ecological perspectives on carbon acquisition in phytoplankton. *Limnol. Oceanogr.* **45**, 744–750 (2000). doi: 10.4319/lo.2000.45.3.0744
110. C. T. Bolton, H. M. Stoll, Late Miocene threshold response of marine algae to carbon dioxide limitation. *Nature* **500**, 558–562 (2013). doi: 10.1038/nature12448; pmid: 23985873
111. M. N. Evans, S. E. Tolwinski-Ward, D. M. Thompson, K. J. Anchukaitis, Applications of proxy system modeling in high resolution paleoclimatology. *Quat. Sci. Rev.* **76**, 16–28 (2013). doi: 10.1016/j.quascirev.2013.05.024
112. G. J. Bowen, B. Fischer-Femal, G. J. Reichart, A. Sluijs, C. H. Lear, Joint inversion of proxy system models to reconstruct paleoenvironmental time series from heterogeneous data. *Clim. Past* **16**, 65–78 (2020). doi: 10.5194/cp-16-65-2020
113. M. B. Osman *et al*., Globally resolved surface temperatures since the Last Glacial Maximum. *Nature* **599**, 239–244 (2021). doi: 10.1038/s41586-021-03984-4; pmid: 34759364
114. C. Godbillot, F. Minoletti, F. Bassinot, M. Hermoso, Parallel between the isotopic composition of coccolith calcite and carbon levels across Termination II: developing a new paleo-CO_2 probe. *Clim. Past* **18**, 449–464 (2022). doi: 10.5194/cp-18-449-2022
115. A. Pack, A. Gehler, A. Süssenberger, Exploring the usability of isotopically anomalous oxygen in bones and teeth as paleo-CO_2-barometer. *Geochim. Cosmochim. Acta* **102**, 306–317 (2013). doi: 10.1016/j.gca.2012.10.017
116. C. R. Scotese, An atlas of Phanerozoic paleogeographic maps: the seas come in and the seas go out. *Annu. Rev. Earth Planet. Sci.* **49**, 679–728 (2021). doi: 10.1146/annurev-earth-081320-064052
117. P. A. Christin, C. P. Osborne, R. F. Sage, M. Arakaki, E. J. Edwards, C_4 eudicots are not younger than C_4 monocots. *J. Exp. Bot.* **62**, 3171–3181 (2011). doi: 10.1093/jxb/err041; pmid: 21393383

ACKNOWLEDGMENTS

We thank C. Major at NSF and the many researchers who contributed advice and enthusiasm for this project over the years. We are grateful to the staff at the National Centers for Environmental Information (NCEI) for facilitating curation of the paleo-CO_2 database, and to LDEO, the UCLA Lake Arrowhead Lodge, and the Lady Bird Johnson Wildflower Center for hosting the three workshops that framed this work. Two anonymous reviewers provided valuable comments that improved this manuscript. This study is dedicated to Wally Broecker and Taro Takahashi, who pioneered the study of CO_2 dynamics in a changing climate. **Funding:** This work was supported by National Science Foundation grant OCE 16-36005 (B.H. and P.J.P.), Heising-Simons Foundation grant 2018-0996 (B.H. and V.F.), National Science Foundation grant EAR 21-21649 (B.H., V.F., J.J.M., and C.F.G.), National Science Foundation grant EAR 21-21170 (G.J.B.), National Science Foundation grant EAR 20-02370 (Y.C.), National Science Foundation grant 18-43285 (A.P.), Columbia University's Center for Climate and Life (K.T.U.), the G. Unger Vetlesen Foundation (K.T.U.), National Science Foundation grant 21-00537 (A.P. and P.J.P.), National Science Foundation grant 21-00509 (P.J.P.), National Science Foundation grant EAR 21-21165 (A.R.), National Science Foundation grant EAR 18-06015 (Y.G.Z.), National Science Foundation grant DGE 16-44869 (S.R.P.), National Science Foundation grant 18-13703 (E.G.H.), National Science Foundation grant OCE 16-58023 (J.C.Z.), National Science Foundation grant 16-02905 (M.H.), Swedish Research Council grant NT7-2016 04905 (M.S.), European Research Council grant 101020824 (J.C.M.), SFI/RC/2092 (J.C.M.), UK Research and Innovation grant 101045371 (M.J.H.), Natural Environment Research Council grant NE/X000567/1 (M.P.S.B.), Royal Society grant DHF\R1\221014 (C.R.W.), Australian Research Council grant DP150104007 (P.J.F.), Deutsche Forschungsgemeinschaft grant RA 2068/4-1 (M.R.), European Research Council grant 805246 (J.W.B.R.), an ETH Fellowship (J.K.C.R.), National Science Foundation of China grant 42030503 (J.D.), the Sandal Society Museum (G.J.R.), a Royal Society Tata Fellowship (B.D.A.N.), and Natural Environment Research Council grant NE/P019048/1 (G.L.F.). **Author contributions:** Conceptualization: B.H., G.J.B., D.O.B., M.J.H., M.J.K., A.P., P.J.P., S.R.P., A.R., D.L.R., M.S., R.S.B., P.J.F., M.H., M.F.S., J.K.C.R., N.D.S., and Y.G.Z. Data curation: B.H., G.J.B., D.O.B., Y.C., M.J.H., M.J.K., J.C.M., P.J.P., D.L.R., M.S., S.R.P., E.A., M.P.S.B., R.S.B., T.B.C., E.d.I.V., K.A.D., C.F.G., M.Gut., D.T.H., L.L.H., T.K.L., M.Gui., J.N.M., R.W., A.R.-N., M.F.S., N.D.S., S.S., C.R.W., Y.G.Z., J.M.C., J.D., D.D.E., G.L.F., E.G.H., B.D.A.N., J.W.B.R., M.R., G.J.R., O.S., and L.Z. Formal analysis: B.H., G.J.B., D.O.B., Y.C., M.J.H., P.J.P., D.L.R., A.M., and C.E.L. Investigation: B.H., D.L.R., D.O.B., P.J.P., S.R.P., G.J.B., M.J.H., Y.C., M.S., J.C.M., M.J.K., A.P., E.A., M.P.S.B., R.S.B., P.J.F., W.K., T.K.L., M.F.S., and Y.G.Z. Software: G.J.B., V.F., J.J.M., and R.W. Visualization: B.H., G.J.B., M.J.H., M.S., J.C.M., K.T.U., P.J.P., D.O.B., J.A., B.A.K., C.R.S., J.J.M., and R.W. Funding acquisition: B.H., P.J.P, D.L.R., D.O.B., G.J.B., M.J.K., A.P., R.M.D., M.H., K.E.S., and V.F. Project administration: B.H., D.L.R., D.O.B., P.J.P., and G.J.B. Writing – original draft: B.H., D.L.R., D.O.B., P.J.P., G.J.B., M.J.H., Y.C., M.S., J.C.M., M.J.K., A.P., K.T.U., A.R., and S.R.P. Writing – review & editing: All authors. **Competing interests:** The authors have no competing interests to declare. **Data and materials availability:** The completed data sheets for each study can be accessed as the paleo-CO_2 "Archive" at NOAA's NCEI (https://www1.ncdc.noaa.gov/pub/data/paleo/climate_forcing/trace_gases/Paleo-pCO2/). The specific choice of category, as well as the updated CO_2 and age estimates, are documented in "Product" sheets for each dataset and proxy. In contrast to the "Archive," which will grow with new publications but will otherwise remain passive, the paleo-CO_2 "Product" is a living database that will be updated when newly published data or ancillary data constraints become available and/or when methodological improvements are developed that enable modernization of previously underconstrained datasets. The "Product" sheets created for this study can be accessed at NCEI (https://www.ncei.noaa.gov/pub/data/paleo/climate_forcing/trace_gases/Paleo-pCO2/product_files/), and this is also the place where future data updates will be made available in consecutive versions of the data "Product." **License information:** Copyright © 2023 the authors, some rights reserved; exclusive licensee American Association for the Advancement of Science. No claim to original US government works. https://www.science.org/about/science-licenses-journal-article-reuse

The CenCO$_2$PIP Consortium

Bärbel Hönisch[1,2], Dana L. Royer[3], Daniel O. Breecker[4], Pratigya J. Polissar[5], Gabriel J. Bowen[6], Michael J. Henehan[7], Ying Cui[8], Margret Steinthorsdottir[9], Jennifer C. McElwain[10], Matthew J. Kohn[11], Ann Pearson[12], Samuel R. Phelps[13], Kevin T. Uno[2], Andy Ridgwell[14], Eleni Anagnostou[15], Jacqueline Austermann[1,2], Marcus P. S. Badger[16], Richard S. Barclay[17], Peter K. Bijl[18], Thomas B. Chalk[19], Christopher R. Scotese[20], Elwyn de la Vega[21], Robert M. DeConto[22], Kelsey A. Dyez[23], Vicki Ferrini[2], Peter J. Franks[24], Claudia F. Giulivi[2], Marcus Gutjahr[15], Dustin T. Harper[6], Laura L. Haynes[25], Matthew Huber[26], Kathryn E. Snell[27], Benjamin A. Keisling[28], Wilfried Konrad[29], Tim K. Lowenstein[30], Alberto Malinverno[2], Maxence Guillermic[31], Luz María Mejía[32], Joseph N. Milligan[17], John J. Morton[2], Lee Nordt[33], Ross Whiteford[34], Anita Roth-Nebelsick[35], Jeremy K. C. Rugenstein[36], Morgan F. Schaller[37], Nathan D. Sheldon[23], Sindia Sosdian[38], Elise B. Wilkes[39], Caitlyn R. Witkowski[7], Yi Ge Zhang[40], Lloyd Anderson[1,2], David J. Beerling[41], Clara Bolton[19], Thure E. Cerling[6], Jennifer M. Cotton[42], Jiawei Da[4], Douglas D. Ekart[43], Gavin L. Foster[44], David R. Greenwood[45], Ethan G. Hyland[46], Elliot A. Jagniecki[47], John P. Jasper[48], Jennifer B. Kowalczyk[49], Lutz Kunzmann[50], Wolfram M. Kürschner[51], Charles E. Lawrence[52], Caroline H. Lear[38], Miguel A. Martínez-Botí[44,53], Daniel P. Maxbauer[54], Paolo Montagna[55], B. David A. Naafs[56], James W. B. Rae[34], Markus Raitzsch[57], Gregory J. Retallack[58], Simon J. Ring[59], Osamu Seki[60], Julio Sepúlveda[61], Ashish Sinha[62], Tekie F. Tesfamichael[63], Aradhna Tripati[31], Johan van der Burgh[64], Jimin Yu[65], James C. Zachos[66], Laiming Zhang[67]

[1]Department of Earth and Environmental Sciences of Columbia University, New York, NY, USA. [2]Lamont-Doherty Earth Observatory of Columbia University, Palisades, NY, USA. [3]Department of Earth and Environmental Sciences, Wesleyan University, Middletown, CT, USA. [4]Department of Earth and Planetary Sciences, Jackson School of Geosciences, University of Texas at Austin, Austin, TX, USA. [5]Department of Ocean Sciences, University of California, Santa Cruz, Santa Cruz, CA, USA. [6]Department of Geology and Geophysics, University of Utah, Salt Lake City, UT, USA. [7]School of Earth Sciences, University of Bristol, Bristol, UK. [8]Department of Earth and Environmental Studies, Montclair State University, Montclair, NJ, USA. [9]Swedish Museum of Natural History, Stockholm, Sweden. [10]Department of Botany, Trinity College Dublin, Dublin, Ireland. [11]Department of Geosciences, Boise State University, Boise, ID, USA. [12]Department of Earth and Planetary Sciences, Harvard University, Cambridge, MA, USA. [13]CIM Group, New York, NY, USA. [14]Earth and Planetary Sciences Department, University of California, Riverside, Riverside, CA, USA. [15]GEOMAR Helmholtz Centre for Ocean Research Kiel, Kiel, Germany. [16]School of Environment, Earth and Ecosystem Sciences, The Open University, Milton Keynes, UK. [17]Department of Paleobiology, Smithsonian Institution, Washington, DC, USA. [18]Department of Earth Sciences, Utrecht University, Utrecht, Netherlands. [19]Aix Marseille University, CNRS, IRD, INRAE, CEREGE, Aix-en-Provence, France. [20]Department of Earth and Planetary Sciences, Northwestern University, Evanston, IL, USA. [21]School of Geography, Archaeology and Irish Studies, University of Galway, Ollscoil na Gaillimhe, Galway, Ireland. [22]Department of

Earth, Geographic, and Climate Sciences, University of Massachusetts, Amherst, MA, USA. [23]Department of Earth and Environmental Sciences, University of Michigan, Ann Arbor, MI, USA. [24]School of Life and Environmental Sciences, The University of Sydney, Sydney, Australia. [25]Department of Earth Science and Geography, Vassar College, Poughkeepsie, NY, USA. [26]Department of Earth, Atmospheric, and Planetary Sciences, Purdue University, West Lafayette, IN, USA. [27]Department of Geological Sciences, University of Colorado Boulder, Boulder, CO, USA. [28]University of Texas Institute for Geophysics, Austin, TX, USA. [29]Department of Geosciences, University of Tübingen, Tübingen, Germany. [30]Department of Earth Sciences, Binghamton University, Binghamton, NY, USA. [31]Department of Earth, Planetary and Space Sciences, University of California, Los Angeles, Los Angeles, CA, USA. [32]MARUM, University of Bremen, Bremen, Germany. [33]Department of Geosciences, Baylor University, Waco, TX, USA. [34]School of Earth and Environmental Sciences, University of St Andrews, St Andrews, UK. [35]State Museum of Natural History, Stuttgart, Germany. [36]Department of Geosciences, Colorado State University, Fort Collins, CO, USA. [37]Department of Earth and Environmental Sciences, Rensselaer Polytechnic Institute, Troy, NY, USA. [38]School of Earth and Environmental Sciences, Cardiff University, Cardiff, UK. [39]Ginkgo Bioworks, Boston, MA, USA. [40]Department of Oceanography, Texas A&M University, College Station, TX, USA. [41]School of Biosciences, University of Sheffield, Sheffield, UK. [42]Department of Geological Science, California State University, Northridge, Northridge, CA, USA. [43]Department of Earth Science, Utah Valley University, Orem, UT, USA. [44]School of Ocean and Earth Science, National Oceanography Centre, University of Southampton, Southampton, UK. [45]Department of Biology, Brandon University, Brandon, Manitoba, Canada. [46]Department of Marine, Earth, and Atmospheric Sciences, North Carolina State University, Raleigh, NC, USA. [47]Utah Geological Survey, Salt Lake City, UT, USA. [48]Nature's Fingerprint Authentication, Molecular Isotope Technologies, LLC, Niantic, CT, USA. [49]Department of Earth, Environmental and Planetary Sciences, Brown University, Providence, RI, USA. [50]Senckenberg Natural History Collections, Dresden, Germany. [51]Department of Geosciences, University of Oslo, Oslo, Norway. [52]Department of Applied Mathematics, Brown University, Providence, RI, USA. [53]EIT Urban Mobility, Barcelona, Spain. [54]Department of Geology, Carleton College, Northfield, MN, USA. [55]Institute of Polar Sciences–National Research Council, Bologna, Italy. [56]School of Chemistry, University of Bristol, Bristol, UK. [57]Dettmer Group KG, Bremen, Germany. [58]Department of Earth Sciences, University of Oregon, Eugene, OR, USA. [59]Deutsches GeoForschungsZentrum GFZ, Potsdam, Germany. [60]Institute of Low Temperature Science, Hokkaido University, Sapporo, Japan. [61]Department of Geological Sciences and Institute of Arctic and Alpine Research, University of Colorado Boulder, Boulder, CO, USA. [62]Department of Earth Science, California State University, Dominguez Hills, Carson, CA, USA. [63]School of Earth Sciences, Addis Ababa University, Addis Ababa, Ethiopia. [64]Independent researcher, Rossum, Netherlands. [65]Laoshan Laboratory, Qingdao, China. [66]Department of Earth and Planetary Sciences, University of California, Santa Cruz, Santa Cruz, CA, USA. [67]Frontiers Science Center for Deep-time Digital Earth, School of Earth Sciences and Resources, China University of Geosciences (Beijing), Beijing, China.

SUPPLEMENTARY MATERIALS

science.org/doi/10.1126/science.adi5177
Supplementary Text
Figs. S1 to S13
Tables S1 to S3
References (*118*–*439*)

Submitted 2 May 2023; accepted 30 October 2023
10.1126/science.adi5177

Toward a Cenozoic history of atmospheric CO_2

The Cenozoic CO2 Proxy Integration Project (CenCO2PIP) Consortium*, Bärbel Hönisch, Dana L. Royer, Daniel O. Breecker, Pratigya J. Polissar, Gabriel J. Bowen, Michael J. Henehan, Ying Cui, Margret Steinthorsdottir, Jennifer C. McElwain, Matthew J. Kohn, Ann Pearson, Samuel R. Phelps, Kevin T. Uno, Andy Ridgwell, Eleni Anagnostou, Jacqueline Austermann, Marcus P. S. Badger, Richard S. Barclay, Peter K. Bijl, Thomas B. Chalk, Christopher R. Scotese, Elwyn de la Vega, Robert M. DeConto, Kelsey A. Dyez, Vicki Ferrini, Peter J. Franks, Claudia F. Giulivi, Marcus Gutjahr, Dustin T. Harper, Laura L. Haynes, Matthew Huber, Kathryn E. Snell, Benjamin A. Keisling, Wilfried Konrad, Tim K. Lowenstein, Alberto Malinverno, Maxence Guillermic, Luz María Mejía, Joseph N. Milligan, John J. Morton, Lee Nordt, Ross Whiteford, Anita Roth-Nebelsick, Jeremy K. C. Rugenstein, Morgan F. Schaller, Nathan D. Sheldon, Sindia Sosdian, Elise B. Wilkes, Caitlyn R. Witkowski, Yi Ge Zhang, Lloyd Anderson, David J. Beerling, Clara Bolton, Thure E. Cerling, Jennifer M. Cotton, Jiawei Da, Douglas D. Ekart, Gavin L. Foster, David R. Greenwood, Ethan G. Hyland, Elliot A. Jagniecki, John P. Jasper, Jennifer B. Kowalczyk, Lutz Kunzmann, Wolfram M. Kürschner, Charles E. Lawrence, Caroline H. Lear, Miguel A. Martínez-Botí, Daniel P. Maxbauer, Paolo Montagna, B. David A. Naafs, James W. B. Rae, Markus Raitzsch, Gregory J. Retallack, Simon J. Ring, Osamu Seki, Julio Sepúlveda, Ashish Sinha, Tekie F. Tesfamichael, Aradhna Tripati, Johan van der Burgh, Jimin Yu, James C. Zachos, and Laiming Zhang

Science **382** (6675), eadi5177. DOI: 10.1126/science.adi5177

Editor's summary

The concentration of atmospheric carbon dioxide is a fundamental driver of climate, but its value is difficult to determine for times older than the roughly 800,000 years for which ice core records are available. The Cenozoic Carbon dioxide Proxy Integration Project (CenCO2PIP) Consortium assessed a comprehensive collection of proxy determinations to define the atmospheric carbon dioxide record for the past 66 million years. This synthesis provides the most complete record yet available and will help to better establish the role of carbon dioxide in climate, biological, and cryosphere evolution. —H. Jesse Smith